Received: 7 August 2020 | Revised: 12 October 2020 | Accepted: 25 November 2020

DOI: 10.4218/etrij.2020-0307

ORIGINAL ARTICLE

ETRI Journal WILEY

Spectrally encapsulated OFDM: Vectorized structure with minimal complexity

Myungsup Kim[1] | **Do Young Kwak**[2] | **Jiwon Jung**[3] | **Ki-Man Kim**[3]

[1]Future Communications Research Laboratory, NEWHIGHTECH, Changwon, Rep. of Korea

[2]Department of Mathematical Sciences, Korea Advanced Institute of Science and Technology, Daejeon, Rep. of Korea

[3]Department of Radio Communications, Korea Maritime and Ocean University, Busan, Rep. of Korea

Correspondence
Jiwon Jung, Department of Radio Communications, Korea Maritime and Ocean University, Busan, Rep. of Korea.
Email: jwjung@kmou.ac.kr

Funding information
This work was supported by the Grant UD200010DD of Agency for Defense Development, Republic of Korea.

To efficiently use frequency resources, the next 6th generation mobile communication technology must solve the problem of out-of-band emission (OoBE) of cyclic prefix (CP) orthogonal frequency division multiplexing (OFDM), which is not solved in 5th generation technology. This study describes a new zero insertion technique to replace an existing filtering scheme to solve this internal problem in OFDM signals. In the development of the proposed scheme, a precoder with a two-dimensional structure is first designed by generating a two-dimensional mapper and using the specialty of each matrix. A spectral shaping technique based on zero insertion instead of a long filter is proposed, so it can be applied not only to long OFDM symbols, but also very short ones. The proposed method shows that the transmitted signal is completely blocked at the bandwidth boundaries of signals according to the current standards, and it is confirmed that the proposed scheme is ideal with respect to bit error rate (BER) performance because its BER is the same as that of CP-OFDM. In addition, the proposed scheme can transformed into a real time structure through vectorizing process with minimal complexity.

KEYWORDS
6G, encapsulation, OFDM, out of band, precoder, spectrum, vectorization

1 | INTRODUCTION

Orthogonal frequency division multiplexing (OFDM) transmission has been used in various fields such as mobile communications [1], wireless local area network (LAN) [2], satellite [3], broadcast [4], and the Internet of Things (IoT) [5] because transmission can be safely made by effectively estimating and correcting multipath channels. However, because the OFDM envelope is a square wave [6], the power spectrum is spread and the out-of-band emission (OoBE) power leaks into adjacent channels [7]. Windowing to smooth the transition of the OFDM envelope has been studied to suppress spectral side lobes [8]. However, the scheme has a disadvantage in that it does not sufficiently suppress OoBE. A general limitation on spectrum precoding of OFDM is defined, and based on this, a block division cyclic prefix (CP)-OFDM scheme has been proposed for spectral efficiency [9] and spectral compactness [10]. The scheme is excellent in terms of performance, but is quite complicated in terms of implementation. The pilot pattern was designed to suppress spectral side lobes in systems that process data and pilot waveforms separately [11]. This method can insert pilots while minimizing the impact on data symbols, but the implementation complexity is rather high. OoBE suppression was first treated as a problem of minimizing the Frobenius norm of the matrix, and an orthogonal precoding scheme

was developed based on singular value decomposition [12]. To eliminate the discontinuity between successive OFDM symbols, the relationship between the previous symbol and the current symbol has been proposed by updating the data vector and the weight vector in a way that reduces the OoBE through differentiation [13]. This method has a recursive structure, and consecutive errors may occur. To reduce the OoBE and the peak-to-average power ratio of OFDM-based systems simultaneously, a method called alignment suppression has been proposed [14]. Because this method uses the original CP in the OFDM symbol, demodulation similar to legacy OFDM can be performed without reducing the transmission efficiency. However, because the transmitter uses channel state information, a secure uplink channel is required, and implementation complexity increases to extract the channel state information from the received signal. In the filter bank multicarrier (FBMC) scheme, each filter bank of a transmission symbol composed of several filter banks is shaped such that the subcarriers reduce OoBE [15]. In general, the symbol length in the filter bank type is more than twice that of conventional OFDM symbols. Therefore, this method cannot be considered suitable for future communication methods that require high transmission efficiency with short delay. A multi-carrier modulation scheme called generalized frequency division multiplexing (GFDM) has been proposed that includes the case of CP-OFDM and single-carrier frequency domain equalization [16]. However, except for the case where the roll-off factor is 0, GFDM has an inherent problem, self-interference, which increases complexity according to the implementation of a receiver that must include an equalization function [17,18]. A filtered OFDM scheme has been proposed that limits the OoBE by filtering OFDM symbols [19,20]. Because the length of the filter is up to half of the length of the OFDM symbol, it may affect the synchronization and bit error rate (BER) performance. A method for reducing OoBE by a transmitter combining conventional OFDM and cancelation carriers has been proposed, and a receiver can demodulate in the same manner as a conventional OFDM demodulation scheme [21]. This scheme has greatly improved spectral characteristics compared to the previous methods [22–24], which have no self-interference, while maintaining the transmission efficiency of the existing OFDM, but it does not completely block the OoBE.

Recently, a technique for completely preventing out-of-band power emission, which is a core technology of future wireless communication technology, has been proposed [25,26]. This technique covered the spectral encapsulation (SE) OFDM technique based on three main techniques: windowing, zero insertion, and orthogonalization. This method was also proposed to completely block OoBE with the short overhead required for encapsulation, instead of using long filters. However, when SE-OFDM [25] is applied to various standards [1–5], the implementation complexity is too high when the fast Fourier transform size is large. This study provides an in-depth analysis of zero insertion, which can be implemented with low complexity and orthogonalization and which has only been proposed by SE-OFDM. The aim is to derive the restoring matrix accurately instead of the orthogonalization matrix in SE-OFDM to significantly reduce implementation complexity. Moreover, this study confirms that the proposed scheme completely blocks the magnitude of the signal at the signal bandwidth boundaries.

Section 2 introduces a generalized structure for a more detailed analysis of SE-OFDM. Section 3 derives accurate and approximate reconstruction matrices, characterizes the matrices, and derives the precoder matrix with the obtained restoring matrix. Section 4 describes the design of a vSE-OFDM transmitter with a reduced vector structure type, calculates the computation amount for generating a vSE-OFDM symbol, and analyzes the frequency response of the precoder in vSE-OFDM. The BER performance of the proposed vSE-OFDM is obtained and analyzed through an additive white Gaussian noise (AWGN) channel and multipath fading channel. Section 5 summarizes the results of the proposed method and suggests how it can be applied to various communication applications in the future.

2 | SE-OFDM

This section introduces the technique of blocking the OoBE by a simple zero insertion method using the SE-OFDM scheme [25]. The SE-OFDM symbol format with prefix and suffix compared to the legacy CP-OFDM symbol is described as shown in Figure 1A. The SE-OFDM symbol format is intended to shape the spectrum without increasing the length of an existing symbol, as suggested in [21]. SE-OFDM is also designed to block the OoBE without degrading the advantages of legacy CP-OFDM. The process for generating a precoder in SE-OFDM consists of five steps, as shown in Figure 1B. In particular, the fifth process, restoration, is discussed separately in Section 3 to identify the properties of the matrix that make up the technique.

The initial mapping matrix $\mathbf{J}\left(\in \mathbb{R}^{N\times M}\right)$ serves to assign input data vectors to predetermined subcarriers as

$$\mathbf{J}=\begin{bmatrix}\mathbf{0}_{\mathrm{dc}} & \\ \mathbf{I}^{+} & \\ & \mathbf{0}_{\mathrm{g}} \\ & \mathbf{I}^{-}\end{bmatrix}, \tag{1}$$

where N and M are the FFT size and the number of data symbols, respectively. In general, the input data symbols are

mapped to each subcarrier, and then the OFDM function is performed through an inverse fast Fourier transform. However, such a method processes signals at the one-dimensional (1D) level mathematically, and it is difficult to expect a more efficient method for blocking OoBE.

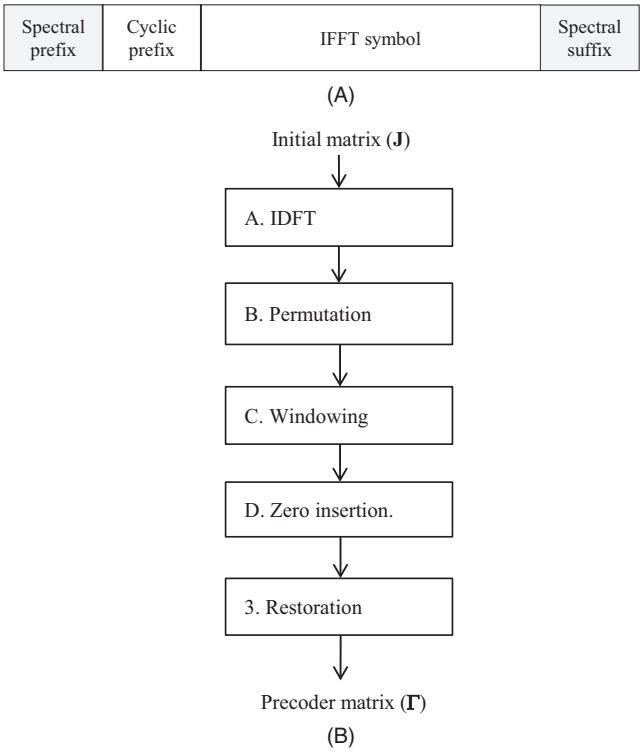

FIGURE 1 SE-OFDM symbol and precoder generation process. (A) SE-OFDM symbol format and (B) precoder generation process. The restoring process is analyzed to significantly reduce the implementation complexity through system analysis in Section 3

The direct current (DC) subcarrier matrix, the positive and negative identity matrices, and the zero guard matrix are, respectively, defined as

$$\mathbf{0}_{\mathrm{dc}} = \mathbf{0}^{\left(1\times\frac{M}{2}\right)}, \tag{2}$$

$$\mathbf{I}^{+} = \mathbf{I}^{-} = \mathbf{I}_{\frac{M}{2}}, \tag{3}$$

$$\mathbf{0}_{\mathrm{g}} = \mathbf{0}^{\left(\beta\times\frac{M}{2}\right)}, \tag{4}$$

where β is the number of guard carriers. Each subcarrier is mapped in a 2D domain for individual processing. Figure 2 shows the initial matrix when the FFT size is eight and the number of subcarriers is six. Because one subcarrier is allocated to each column, independence is maintained between subcarriers. In other words, $\mathbf{J}^{\mathrm{H}}\mathbf{J} = \mathbf{I}_M$.

2.1 | IDFT (inverse discrete Fourier transform)

The discrete Fourier transform (DFT) matrix is defined as

$$\mathbf{F}_N = \frac{1}{\sqrt{N}}\left[e^{-j\frac{2\pi kl}{N}}\right]_{-\frac{N}{2}\le k,l\le\frac{N}{2}-1}, \tag{5}$$

and the time domain carrier matrix is represented as

$$\mathbf{P} = \mathbf{F}_N^{\mathrm{H}}\mathbf{J}. \tag{6}$$

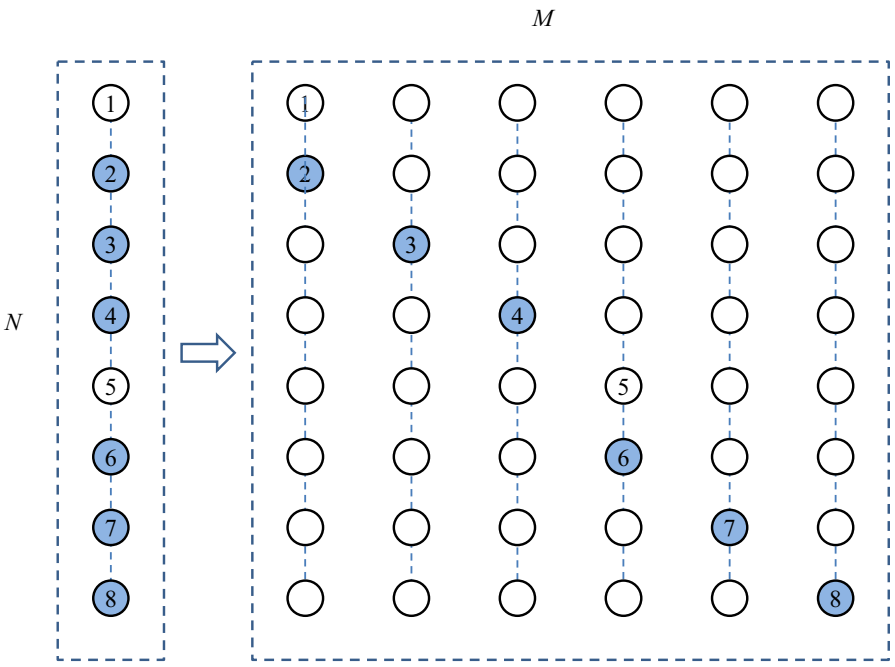

FIGURE 2 Mapping matrix $\mathbf{J}$ with $M = 6$, $N = 8$. (A) 1D mapping and (B) 2D mapping. The aim of 2D mapping is to enable independent processing of each subcarrier evenly distributed over the entire band

2.2 | Permutation

The permutation matrix is defined as

$$\mathbf{E} = \begin{bmatrix} & & \mathbf{I}_{\lceil L_{\mathrm{p}} - \frac{r}{2} \rceil} \\ & \mathbf{I}_{L_{\mathrm{cp}}} & \\ \mathbf{I}_N & & \\ & \mathbf{I}_{\lfloor L_{\mathrm{s}} - \frac{r}{2} \rfloor} & \end{bmatrix}, \tag{7}$$

where L_{p}, L_{cp}, and L_{s} are the lengths of the prefix, CP, and suffix, respectively, and r is the order of the binomial filter, to be defined later.

The permuted matrix is

$$\mathbf{Q} = \mathbf{EP} = \begin{bmatrix} \mathbf{Q}_p \\ \mathbf{P}_{cp} \\ \mathbf{P} \\ \mathbf{Q}_s \end{bmatrix}, \tag{8}$$

where $\mathbf{Q} \in \mathbb{C}^{(L-r)\times M}$ and $L = L_{\mathrm{p}} + L_{\mathrm{cp}} + N + L_{\mathrm{s}}$.

2.3 | Windowing

The windowing matrix is defined as a diagonal matrix

$$\mathbf{W} = \mathrm{diag}\left(\left[\varsigma_1, \ldots, \varsigma_{L_{\mathrm{p}} - \frac{r}{2}}, \overbrace{1, 1, \ldots, 1,}^{L_{\mathrm{cp}}+N} \varsigma_{L_{\mathrm{s}} - \frac{r}{2}}, \ldots, \varsigma_1 \right] \right) \tag{9}$$

and the windowed matrix is

$$\mathbf{R} = \mathbf{WQ} = \begin{bmatrix} \mathbf{R}_{\mathrm{p}} \\ \mathbf{P}_{\mathrm{cp}} \\ \mathbf{P} \\ \mathbf{R}_{\mathrm{s}} \end{bmatrix}, \tag{10}$$

where $\mathbf{R} \in \mathbb{C}^{(L-r)\times M}$. The vector $\left[\varsigma_1, \ldots, \varsigma_{L_{\mathrm{p}} - \frac{r}{2}}, \varsigma_{L_{\mathrm{p}} - \frac{r}{2}}, \ldots, \varsigma_1 \right]$ that expresses the transition signal usually uses a raised cosine function.

2.4 | Zero insertion

In general, to completely remove OoBE, a filter with a very large number of taps should be used. However, because such a method requires a large amount of computation and has a long filter response, it becomes longer than the original OFDM symbol, which may reduce transmission efficiency or cause interference in neighboring symbols. This subsection proposes a technique that completely blocks the power leakage of a signal by inserting zeros at the band boundaries of the signal using a very simple filter. Of course, because the filter is very simple, it may not have a flat characteristic in the pass band and distortion may occur. Zero insertion at the bandwidth boundary of the signal is performed through a binomial filter. The binomial filter performs the function of making the signal size 0 at the boundary. Because the length of the binomial filter is very short (2 or 3), distortion occurs within the pass bandwidth that must be passed. However, in this study, the signal is restored through the restoration process described in Section 3 so that the distortion in the passband has the original flat characteristics. That is, the restoration function is performed through restoring matrix X. This issue is addressed in the next section by a restoring matrix that returns the IFFT symbol part to its original IFFT symbol. This technique is very different from the conventional method of limiting the spectrum through a long filter, and it can block out-of-band power leakage with a very short filter as follows. We define a $L \times (L - r)$ zero-insertion matrix as

$$\mathbf{C} = \begin{bmatrix} c_0 & & & \\ \vdots & c_0 & & \\ c_r & \vdots & & \\ & c_r & \ddots & c_0 \\ & & & \vdots \\ & & & c_r \end{bmatrix}, \tag{11}$$

$$c(z) = \frac{1}{2^r}\left(1 + z^{-1}\right)^r, \tag{12}$$

which is based on the r-th order binomial function [27] and which has zeros at the bandwidth boundaries. The zero-inserted matrix is

$$\mathbf{G} = \mathbf{CR}. \tag{13}$$

3 | RESTORATION

The inner blocks $\mathbf{G}_{\mathrm{cp}}$ and $\mathbf{G}_{\mathrm{c}}$ in $\mathbf{G}$ formed by multiplying convolution matrix $\mathbf{R}$ by matrix $\mathbf{C}$ are distorted by matrix $\mathbf{C}$, so they should be restored to the original $\mathbf{P}_{\mathrm{cp}}$ and $\mathbf{P}$, respectively. We derive the exact restoring matrix for SE-OFDM and analyze its properties. The precoder matrix can be obtained by multiplying matrix $\mathbf{G}$ by restoring matrix $\mathbf{X}$ as

$$\Gamma = \mathbf{GX} = \begin{bmatrix} \mathbf{G}_{\mathrm{p}} \\ \mathbf{G}_{\mathrm{cp}} \\ \mathbf{G}_{\mathrm{c}} \\ \mathbf{G}_{\mathrm{s}} \end{bmatrix} \mathbf{X}. \tag{14}$$

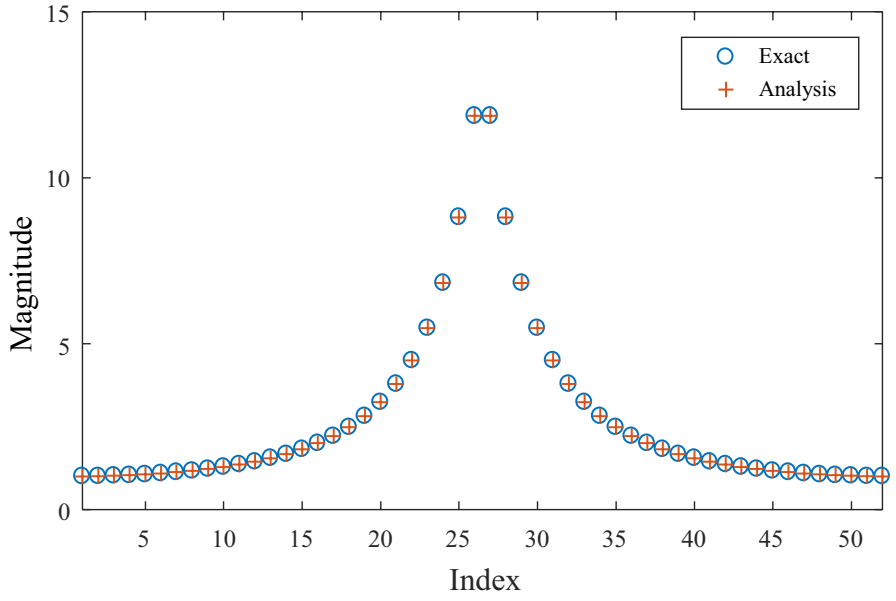

FIGURE 3 Diagonal vectors of restoring matrices with $\beta = 11$, $L_p = L_s = 8$, $L_{cp} = 8$, $M = 52$, and $N = 64$

The CP-OFDM symbol located in the center of the vSE-OFDM symbol transmitted in the proposed scheme is transmitted without change by the precoder. In other words, the IFFT symbol is not affected by the precoder. Restoration is the process of returning the information transmission part changed by zero insertion to the original orthogonal matrix as

$$\begin{bmatrix} \mathbf{G}_p \\ \mathbf{G}_{cp} \\ \mathbf{G}_c \\ \mathbf{G}_s \end{bmatrix} \mathbf{X} = \begin{bmatrix} \mathbf{G}_p\mathbf{X} \\ \mathbf{P}_{cp} \\ \mathbf{P} \\ \mathbf{G}_s\mathbf{X} \end{bmatrix}. \tag{15}$$

From Appendix A, we have the solution

$$\mathbf{X} = \mathbf{G}_c^{+}\mathbf{P}. \tag{16}$$

From Appendix B, we also obtain another solution:

$$\mathbf{X} = \left(\mathbf{G}_c^{H}\mathbf{G}_c\right)^{-\frac{1}{2}}, \tag{17}$$

which is the restoring matrix that makes the center precoder orthogonal.

From (15), we have

$$\mathbf{G}_c\left(\mathbf{G}_c^{H}\mathbf{G}_c\right)^{-\frac{1}{2}} = \mathbf{P}, \tag{18}$$

which is the relation between $\mathbf{G}_c$ and $\mathbf{P}$.

The center matrix is represented as a filtered form as

$$\mathbf{G}_c = \left[\mathbf{c} * \mathbf{r}_1, \mathbf{c} * \mathbf{r}_2, \ldots, \mathbf{c} * \mathbf{r}_M\right]_{N\times M}, \tag{19}$$

where

$$\mathbf{c} = \left[c_0, \ldots, c_r\right]^T, \tag{20}$$

$\mathbf{r}_i$ is the i-th column of $\mathbf{R}$, $*$ denotes the convolution operator, and $[\mathbf{A}]_{N\times M}$ denotes the size-reduced matrix of $\mathbf{A}$.

From Appendix C, we can represent the matrix $\mathbf{G}_c$ in the frequency domain as

$$\hat{\Psi} = \begin{bmatrix} \mathbf{0}_{1\times M} \\ \mathbf{A} \\ \mathbf{0}_{\beta\times M} \\ \mathbf{B} \end{bmatrix}, \tag{21}$$

where

$$\mathbf{A} = \begin{bmatrix} \gamma_1 & & & \\ & \gamma_2 & & \\ & & \ddots & \\ & & & \gamma_{M/2} \end{bmatrix}, \tag{22}$$

$$\mathbf{B} = \begin{bmatrix} \gamma_{N+2-M/2+1} & & & \\ & \gamma_{N+2-M/2+2} & & \\ & & \ddots & \\ & & & \gamma_{N+2} \end{bmatrix}, \tag{23}$$

and γ_i is the i-th entry of $\boldsymbol{\gamma}$.

The time domain representation of $\hat{\Psi}$ is obtained through IDFT as

$$\mathbf{G}_c \approx \mathbf{F}_N^{H}\hat{\Psi}. \tag{24}$$

Substituting (24) into (17) yields

$$\begin{aligned}\mathbf{X} &\approx \left(\left(\mathbf{F}_N^H\hat{\Psi}\right)^H\mathbf{F}_N^H\hat{\Psi}\right)^{-\frac{1}{2}}\\ &= \left(\hat{\Psi}^H\mathbf{F}_N\mathbf{F}_N^H\hat{\Psi}\right)^{-\frac{1}{2}}\\ &= \left(\hat{\Psi}^H\hat{\Psi}\right)^{-\frac{1}{2}}.\end{aligned} \tag{25}$$

From Appendix D, we have

$$\mathbf{X} \approx \begin{bmatrix}\mathbf{A}^{-1} & \mathbf{0}\\ \mathbf{0} & \mathbf{B}^{-1}\end{bmatrix}. \tag{26}$$

Therefore, it can be seen that the approximated matrix of $\mathbf{X}$ is Hermitian and diagonal. Figure 3 shows the exact diagonal elements by (16) and the approximate diagonal elements by (26). The two dotted curves are in good agreement, confirming that (26) is close to (16).

Substituting (16) into (14), the precoder matrix becomes

$$\Gamma = \begin{bmatrix}\Gamma_{\mathrm{p}}\\ \mathbf{P}_{\mathrm{cp}}\\ \mathbf{P}\\ \Gamma_{\mathrm{s}}\end{bmatrix}, \tag{27}$$

where

$$\Gamma_{\mathrm{p}} = \mathbf{G}_{\mathrm{p}}\mathbf{X} = \mathbf{G}_{\mathrm{p}}\mathbf{G}_{\mathrm{c}}^{+}\mathbf{P}, \tag{28}$$

$$\Gamma_{\mathrm{s}} = \mathbf{G}_{\mathrm{t}}\mathbf{X} = \mathbf{G}_{\mathrm{t}}\mathbf{G}_{\mathrm{c}}^{+}\mathbf{P}. \tag{29}$$

The precoder generation process is depicted in Figure 4. The operator $\otimes_{\mathrm{r}}$ denotes right multiplication.

From Figure 4, the precoder is represented as

$$\Gamma = \mathbf{CWEF}_N^{\mathrm{H}}\mathbf{JX}. \tag{30}$$

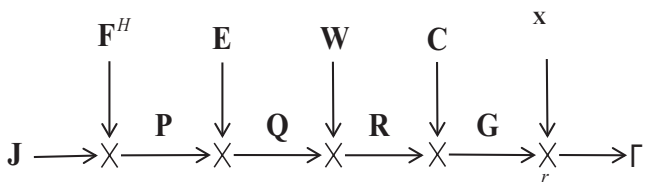

FIGURE 4 Signal flow diagram for generation of a precoder matrix

3.1 | Bandwidth of the precoder

The precoder can be written in a convolution form as

$$\begin{aligned}\Gamma &= \mathbf{CY}\\ &= \left[\mathbf{c}*\mathbf{y}_{1,}\ \mathbf{c}*\mathbf{y}_{2,}\ \ldots,\mathbf{c}*\mathbf{y}_{M}\right],\end{aligned} \tag{31}$$

where $\mathbf{Y} = \mathbf{WE}_{\mathrm{p}}\mathbf{F}_N^{\mathrm{H}}\mathbf{JX}$ and $\mathbf{y}_i$ is the i-th column of $\mathbf{Y}$. Each column of the precoder is represented by a convolution of the vectors $\mathbf{c}$ and $\mathbf{y}_i$, which means that all of the precoder columns are filtered by the zero insertion filter, and the bandwidth of the precoder is confined by the zero insertion filter. Thus, the precoded signal becomes zero at the bandwidth boundaries, regardless of $\mathbf{Y}$ in the frequency domain.

4 | VECTORIZATION

4.1 | Vectorized structure

With the proposed precoder, the transmitted symbol is represented as

$$\mathbf{s} = \Gamma\mathbf{d}, \tag{32}$$

where $\mathbf{d} = \left[d_1, d_{2,}\ \ldots, d_M\right]^T$ is a data symbol vector, and each entry $d_i\left(i = 1, 2, \ldots, M\right)$ is an M-ary QAM symbol.

From Appendix E, we have

$$\mathbf{s} = \mathbf{c} * \left(\mathbf{wE}\,\mathbf{F}_N^{\mathrm{H}}\mathbf{Jx} \odot \mathbf{d}\right), \tag{33}$$

where $\odot$ is the element-wise product operator.

From (33), we have vectorized precoder

$$\boldsymbol{\zeta} = \mathbf{c} * (\Pi\mathbf{x}), \tag{34}$$

where

$$\boldsymbol{\Pi} = \mathbf{WEF}_N^{\mathrm{H}}\mathbf{J}, \tag{35}$$

which is the OFDM core.

The OFDM symbol generation processes of SE-OFDM and vSE-OFDM are shown in Figure 5A,B, respectively. In the SE-OFDM scheme, as the IFFT size increases, the size of the precoder matrix increases as the square. Therefore, it is easy to apply to short OFDM symbols, but difficult to apply to long OFDM symbols.

In the vSE-OFDM scheme, the OFDM transmitter core and the IEEE 802.11 g specification [28] with a windowing scheme

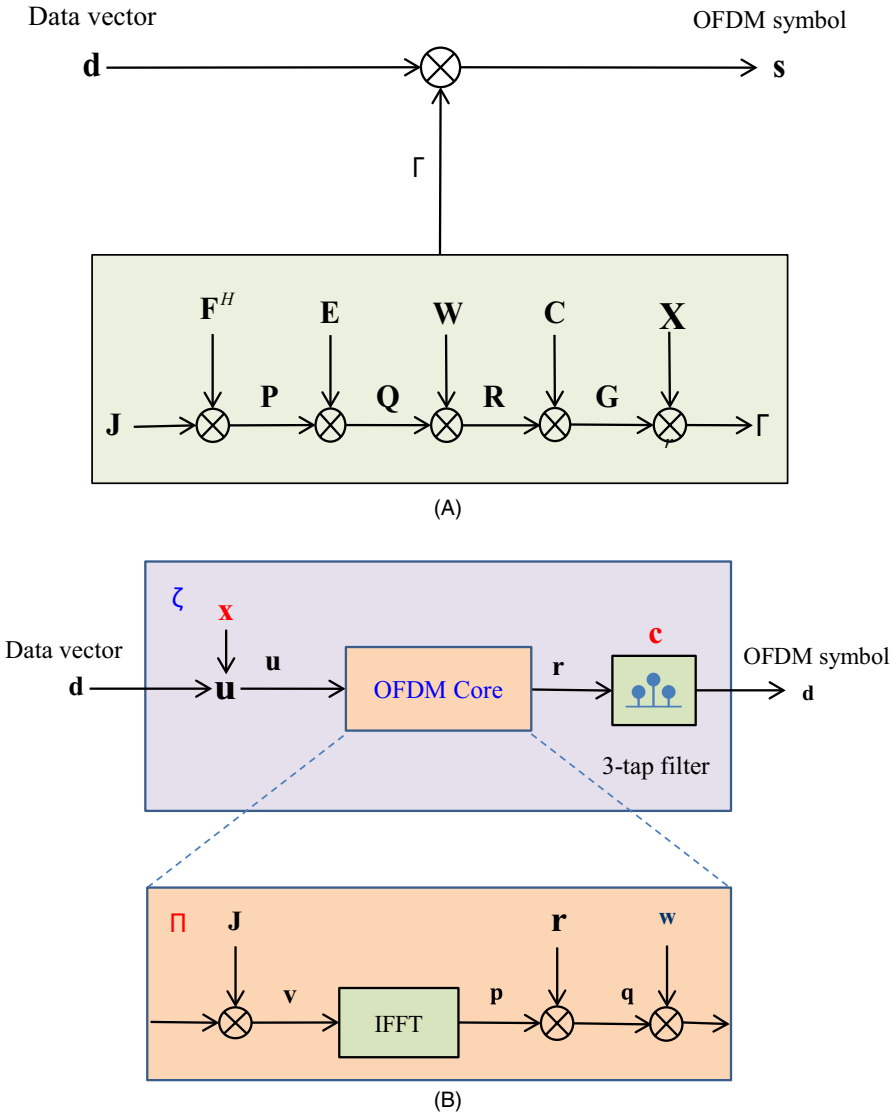

FIGURE 5 Block diagrams of two spectrally efficient precoding schemes. (A) SE-OFDM and (B) vSE-OFDM

are included. There is an element-wise product of vector **d** and vector **x** at the input stage and at the filter that performs zero insertion. The implementation complexity of the vSE-OFDM transmitter can be significantly reduced by vectorization. The vSE-OFDM scheme has a simple structure because it includes the OFDM core with an IFFT processor, as shown in Figure 5B. Matrices **J** and **E** act as mapping and permutation matrices, respectively, so no multiplication is required during operation. In particular, when $r = 2$, the elements of **x** are real, and we can design a precoder with minimal complexity. It can be seen that this model can completely block OoBE in a vector **x** and a 3-tap filter regardless of the OFDM core.

In the process of generating an OFDM symbol in the vSE-OFDM scheme using IFFT, the ratio of multipliers of vSE-OFDM compared to legacy OFDM is greatly reduced from

$$\rho_{\mathrm{SE}} = \frac{M}{D}\left(L_{\mathrm{p}} + L_{\mathrm{cp}} + N + L_{\mathrm{s}}\right), \tag{36}$$

to

$$\rho_{\mathrm{vSE}} = \begin{cases} \dfrac{M+r+1}{D} & r = \text{odd}, \\ \dfrac{\frac{M}{2}+r+1}{D} & r = \text{even}, \end{cases} \tag{37}$$

where

$$D = N\log_2 N + \frac{1}{2}\left(L_{\mathrm{p}} + L_{\mathrm{s}}\right). \tag{38}$$

When r is even, the numerator becomes $M/2$ instead of M because the vector **x** consists of real entries. The term $\left(L_{\mathrm{p}} + L_{\mathrm{s}}\right)/2$ instead of $L_{\mathrm{p}} + L_{\mathrm{s}}$ in (38) is because windowing prefix and suffix require real multiplications.

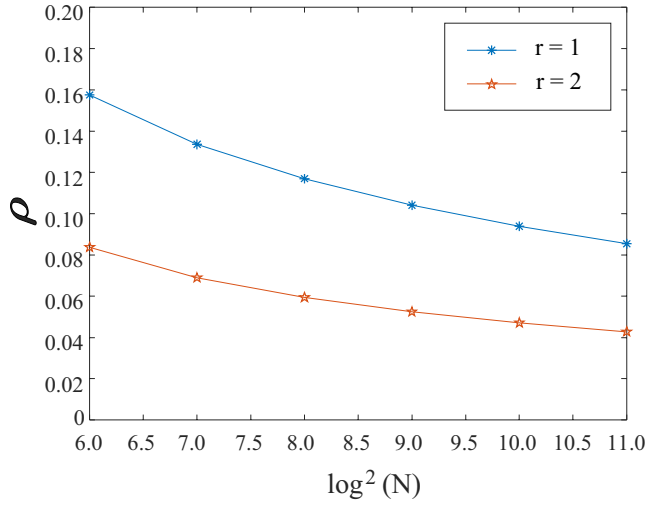

FIGURE 6 Additional multiplier ratio of vSE-OFDM with respect to CP-OFDM

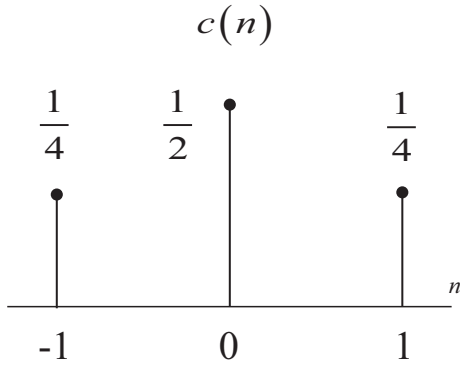

FIGURE 7 Coefficients of the binomial filter with $r = 2$

Figure 6 shows the normalized amount of additional multipliers needed to accommodate vSE-OFDM with respect to the amount of OFDM core. Additional amounts are shown for $N = 64$, 128, 256, 1024, 2048, and $M = 0.96N$. When $N = 64$, the additional amounts are 0.16 and 0.082, respectively, for $r = 1$ and 2. In contrast, when $N = 2048$, the additional amounts are reduced considerably to 0.082 and 0.041, respectively, for $r = 1$ and 2. Overall, when $r = 2$, it is shown that an increase in the number of multipliers within 10% can completely block the OoBE. When $r = 1$, the filter has a minimal length of 2, and when $r = 2$, the filter has a length of 3 and the entries of vector **x** can be real. In Figure 6, when $r = 2$, that is, when the length of the filter is 3, the additional calculation amount is 10% (0.1) or less regardless of the IFFT length N, indicating that OoBE can be completely blocked. In the case of [29], which is a combination of existing methods, it can be seen that the proposed method is better the method that requires more than 200% of the computational amount compared to the original method.

A binomial filter can be configured symmetrically around n = 0, as shown in Figure 7. Because such a filter is a symmetric function, it is a real function in the frequency domain. In other words, when $r = 2$, the vector **x** becomes a real vector and the amount of computation for a transmitter is less than when $r = 1$.

In the implementation, the cyclic prefix and the suffix length may be adjusted to maintain compatibility with conventional OFDM in terms of symbol length. The proposed technique is innovative in terms of spectral shaping because it can completely block the spectrum with a 2-tap digital filter. In other words, the minimum length of the digital filter required to completely block OoBE is 2.

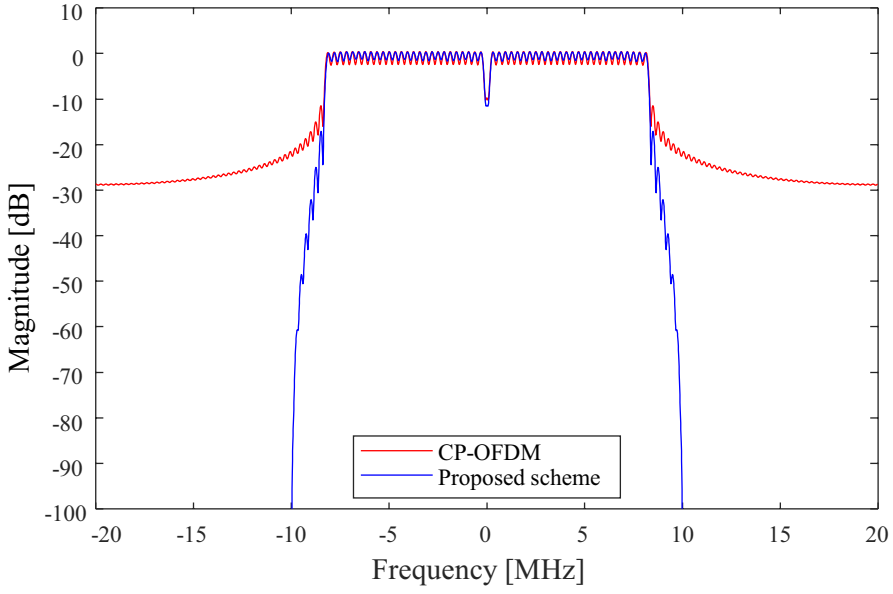

FIGURE 8 Frequency responses of CP-OFDM and vSE-OFDM with $\beta = 11$, $L_p = L_s = 8$, $L_{cp} = 8$, $M = 52$, $N = 64$, $c(z) = (1 + 2z^{-1} + z^{-2})/4$

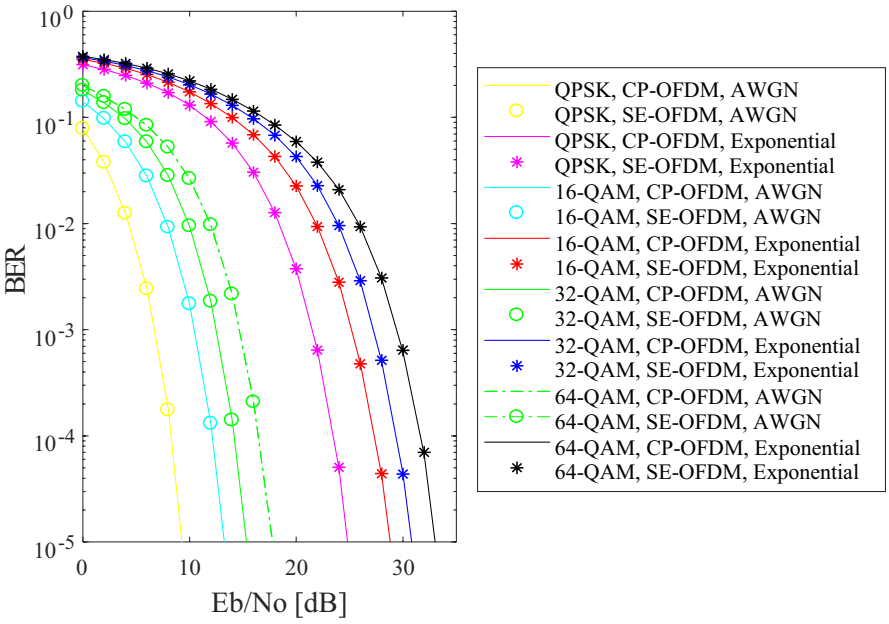

FIGURE 9 BER performance ($M = 244$, $N = 256$, $\beta = 11$, $r = 2$). The label "Exponential" indicates the exponential channel given by $h(k)$

4.2 | Frequency response

The frequency characteristics of CP-OFDM and vSE-OFDM, which include the information transmission part as in the existing CP-OFDM, are shown in Figure 8. At the boundaries of the frequency bands of −10 MHz and 10 MHz, the signal is completely blocked, but the passband characteristics of SE-OFDM appear to be the same as those of CP-OFDM. The frequency-blocking characteristic is good even when the SE-OFDM scheme is applied to very short OFDM symbols of 64 FFT size according to the IEEE 802.11a standard [30]. Figure 5B shows that the OoBE can be completely blocked using a very short filter with three taps, which is a major characteristic of the proposed vSE-OFDM. Thus far, there has been no published method that completely blocks OoBE using such a short filter. Of course, the vSE-OFDM scheme can also be applied to long OFDM symbols and can be implemented more easily than any existing OoBE blocking schemes.

4.3 | BER performance

We show that vSE-OFDM has been faithfully modified without degrading the original BER performance of SE-OFDM. Because, except for the OoBE problem, CP-OFDM has an ideal BER performance, we compare the performance of the proposed vSE-OFDM method with that of CP-OFDM through the AWGN channel and the multipath delay fading channel $h(k) = C \cdot 10^{-k/10}, k = 0, 1, \ldots, 31$ [31] to obtain the BER performance, where C is the power normalization factor.

The proposed method's BER performance is evaluated by receiving OFDM symbols modulated with quadrature phase shift keying (QPSK), 32-QAM, and 64-QAM over two types of channels. As shown in Figure 9, it is confirmed that the performance of vSE-OFDM proposed in the AWGN channel matches the performance of the ideal CP-OFDM. Therefore, it can be seen that the IFFT symbol among the precoded OFDM symbols is not affected in the precoding process. In addition, because the performance of the proposed vSE-OFDM scheme over the multipath delay fading channel is consistent with that of CP-OFDM, this indicates that the IFFT symbol is not changed in the vSE-OFDM scheme. By vectorizing the SE-OFDM method, it was confirmed that the newly configured vSE-OFDM transmitter matches the transmitter of SE-OFDM. With respect to BER, it is confirmed that the performances of CP-OFDM and the proposed vSE-OFDM scheme are consistent in four modulation schemes and two channel environments, which means that vectorization has been successfully achieved. The vSE-OFDM completely blocks OoBE from the OFDM signal through a vector structure filter, as shown in Figure 8. Therefore, the original OFDM performance should not be damaged. Figure 9 shows that vectorization was successful because the BER performance of the proposed schemes vSE-OFDM and CP-OFDM match.

Calculating the amount of computation for each method can be performed by looking at the nature of the spectrum limiting algorithm. To date, many proposed OoBE blocking methods that cause interference between subcarriers at the transmitting side and equalize at the receiver cannot be evaluated sufficiently. The reason is that shaping the transmit spectrum is a problem with the transmitter and there is no reason to intervene all the way to the receiver. Even if an equalizer is used, compensation according to the channel conditions can become a serious problem. Therefore, a method in which the receiver did not require an equalizer was evaluated as low in

TABLE 1 Scheme-specific characteristics

Scheme	Self-interference	Equalizer	Spectral blocking	Implementation complexity	BER
OFDM	NE	NR	Low	Low Low	Ideal
SP-OFDM [10]	NE	NR	High	Low High	Good
O-Precoding [12]	NE	NR	High	Low Medium	Good
N-OFDM [13]	NE	NR	High	Low Medium	Good
FBMC [15]	EX	RQ	High	Low High	Good
E-GFDM [17]	EX	RQ	High	Low High	Good
F-OFDM [19]	EX	RQ	High	Low High	Good
GSS-OFDM [21]	NE	NR	High	Low Medium	Ideal
SE-OFDM [25]	NE	NR	Nearly Perfect	Low Medium	Nearly ideal
Proposed vSE-OFDM	NE	NR	Perfect	Medium Low	Ideal

Abbreviations: EX, existence; NE, nonexistence; Nearly Ideal, not mathematically ideal, but engineering ideal; Nearly Perfect, not mathematically perfect, but engineering perfect; NR, not required; Perfect, the magnitude of the signal is zero at the signal bandwidth boundaries; RQ, required.

complexity. In addition, the method of increasing the sampling rate to limit the spectrum cannot be viewed as a method suitable for a future era that requires high-speed communication. The scheme proposed in this paper is designed to maintain perfect spectrum blocking and transmission performance with a minimum amount of computation without compromising the advantages of the current OFDM scheme CP-OFDM.

In F-OFDM [19], the receiver has a similar performance to that of CP-OFDM through equalization. However, the proposed method can be implemented more simply than F-OFDM because the transmission method does not cause distortion by the precoder at the receiver, so an equalizer is not required. E-GFDM [12] was developed to improve BER performance to the same level as CP-OFDM by eliminating self-interference. However, this method is inferior to the proposed vSE-OFDM method in terms of spectral characteristics and BER performance. Table 1 summarizes the results analyzed so far. The implementation complexity is classified according to the structures of the transmitter and receiver.

5 | CONCLUSION

This study addressed how to create a new precoder for complete OoBE blocking for next 6th generation mobile communication technologies. The restoring matrix in the precoder was identified to be a diagonal matrix, and based on this matrix, a new vector type precoder for OFDM symbol generation was constructed. The newly proposed vSE-OFDM includes legacy CP-OFDM, and one vector and a 3-tap filter can completely block OoBE with minimal operations, unlike the existing filtering-based method. Even if the IFFT size is as large as 2048, setting $r = 2$ indicates that OoBE can be completely blocked when the amount of additional calculation is less than 5% compared to the existing CP-OFDM method, which shows that the short time response and OoBE blocking characteristics are superior to any of the methods suggested so far. Because the proposed vSE-OFDM has no self-interference, it is compatible with various communication standards such as broadcasting, satellite communication, wireless LAN, the Internet of Things, and mobile communication.

ORCID

Myungsup Kim https://orcid.org/0000-0003-3344-2545

REFERENCES

1. ETSI TS 136 101 v10.3.0 Release 10, LTE; Evolved universal terrestrial radio access (E-UTRA); User equipment (UE) radio transmission and reception (3GPP TS 36.101 version 10.3.0 Release 10), ETSI TS, Sophia Antipolis, 2011.
2. IEEE 802.11-15/0132r15, Specification framework for TGax, IEEE 802.11, Hillsboro, 2016.
3. A. Papathanassiou, A. K. Salkintzis, and P. T. Mathiopoulos, *A comparison study of the uplink performance of W-CDMA and OFDM for mobile multimedia communications via LEO satellites*, IEEE Personal Commun. **8** (2001), 35–43.
4. EN 302304 v1.1.1, Digital video broadcasting (DVB), transmission system for handheld terminals (DVB-H), EN, Sophia Antipolis, 2004.
5. L. Cho et al., *Green OFDM for IoT: Minimizing IBO subject to a spectral mask*, in Proc. IEEE Int. Conf. Appl. Syst. Invent. (ICASI), (Chiba, Japan), Apr. 2018, pp. 13–17, https://doi.org/10.1109/ICASI.2018.8394252
6. D. Qu et al., *Detection of non-contiguous OFDM symbols for cognitive radio systemswithout out-of-band spectrum synchronization*, IEEE Trans. Wirel. Commun. **10** (2011), 693–701.
7. A. Sahin, I. Güvenç, and H. Arslan, *A survey on multicarrier communications: Prototype filters, lattice structures, and implementation aspects*, IEEE Commun. Sur. Tut. **16** (2014), 1312–1338.
8. A. Sahin and H. Arslan, *Edge windowing for OFDM based systems*, IEEE Commun. Lett. **15** (2011), 1208–1211.

9. C.-D. Chung, *Spectral precoding for rectangular pulsed OFDM*, IEEE Trans. Commun. **59** (2008), 1498–1510.
10. C.-D. Chung and K.-W. Chen, *Spectrally precoded OFDM without guard insertion*, IEEE Trans. Veh. Technol. **66** (2017), 107–121.
11. W.-C. Chen and C.-D. Chung, *Spectrally efficient OFDM pilot waveform for channel estimation*, IEEE Trans. Commun. **65** (2017), 387–402.
12. M. Ma et al., *Optimal orthogonal precoding for power leakage suppression in DFT-based systems*, IEEE Trans. Commun. **59** (2011), 387–402.
13. J. van de Beek and F. Berggren, *N-continuous OFDM*, IEEE Commun. Lett. **13** (2009), 1–3.
14. A. Tom, A. Şahin, and H. Arslan, *Suppressing alignment: Joint PAPR and out-of-band power leakage reduction for OFDM-based systems*, IEEE Trans. Commun. **64** (2016), 1100–1109.
15. B. Farhang-Boroujeny, *OFDM versus filter bank multicarrier*, IEEE Signal Process. Mag. **28** (2011), 92–112.
16. R. Datta et al., *GFDM interference cancellation for flexible cognitive radio PHY design*, in Proc. IEEE Veh. Technol. Conf. (Quebec City, Canada), Sept. 2012, pp. 1–5.
17. J. K. Jeong et al., *Eigendecomposition-based GFDM for interference-free data transmission and pilot insertion for channel estimation*, IEEE Trans. Wirel. Commun. **17** (2018), 6931–6943.
18. F. Li et al., *Design and performance of a novel interference-free GFDM transceiver with dual filter*, IEEE Trans. Veh. Technol. **68** (2019), 3045–3061.
19. J. Abdoli, M. Jia, and J. Ma, *Filtered OFDM, a new waveform for future wireless systems*, in Proc. IEEE Int. Workshop Signal Process. Adv. Wirel. Commun. (Stockholm, Sweden), June 2015, https://doi.org/10.1109/SPAWC.2015.7227001
20. H. Chen et al., *Interference analysis in the asynchronous f-OFDM systems*, IEEE Trans. Commun. **67** (2019), 3580–3596.
21. L. Díez et al., *A generalized spectral shaping method for OFDM signals*, IEEE Trans. Commun. **67** (2019), 3540–3551.
22. J. A. C. Bingham, *RFI suppression in multicarrier transmission systems*, in Proc. IEEE Glob. Telecommun. Conf. (London, UK), Nov. 1996, pp. 1026–1030.
23. T. Weiss et al., *Mutual interference in OFDM-based spectrum pooling systems*, in Proc IEEE Veh. Technol. Conf. (Milan, Italy), May 2004, pp. 1873–1877.
24. D. Qu, A. Wang, and T. Jiang, *Extended active interference cancellation for sidelobe suppression in cognitive radio OFDM systems with cyclic prefix*, IEEE Trans. Veh. Tech. **59** (2010), 1689–1695.
25. M. S. Kim et al., *Spectral encapsulation of OFDM systems based on orthogonalization for short packet transmission*, ETRI J. **42** (2020), 1–13.
26. M. S. Kim et al., *Spectral encapsulation to block the out-of-band emission of OFDM signals for future communications*, in Proc. IEEE Veh. Technol. Conf. (VTC2020-Spring) (Antwerp, Belgium), May 2020, pp. 1–5, https://doi.org/10.1109/VTC2020-Spring48590.2020.9129421
27. M. S. Kim et al., *Multinomial filter*, in Proc. Int. Conf. Inform. Commun. Technol. Convergence (ICTC) (Busan, Rep. of Korea), Oct. 2014, pp. 819–823, https://doi.org/10.1109/ICTC.2014.6983301
28. IEEE Std. 802.11gTM, Wireless LAN medium access control and physical layer specifications, higher speed physical layer (PHY) extension in the 5GHz band, 2003.
29. Z. You, J. Fang, and I. Lu, *Out-of-band emission suppression techniques based on a generalized OFDM framework*, EURASIP J. Adv. Signal Process. **74** (2014), 1–14.
30. IEEE Std. 802.11a/D5.0, Wireless LAN medium access control and physical layer specifications, higher speed physical layer extension in the 5GHz band, 1999.
31. N. Michailow et al., *Generalized frequency division multiplexing for 5th generation cellular networks*, IEEE Trans. Commun. **62** (2014), 3045–3061.

AUTHOR BIOGRAPHIES

Myungsup Kim received his BS degree in electronic engineering from Han Yang University, Seoul, Republic of Korea, in 1986, his MS in electronic engineering from Chungnam National University, Republic of Korea, in 1991, and his PhD degree in information and communication engineering from the Korea Advanced Institute of Science and Technology (KAIST), Seoul, Republic of Korea, in 1999. From 1986 to 2000, he worked for the Electronics and Telecommunications Research Institute, Daejeon, Republic of Korea. From 2001 to 2014, he worked for Tunitel Co., Daejeon, Republic of Korea. From 2015 to 2019, he worked for the Department of Mathematical Sciences, KAIST, Daejeon, Republic of Korea. Since 2020, he has been working for NEWHIGHTECH, Changwon, Republic of Korea, where he is now a research director. His main research interests include communication theory and signal processing for future wireless and underwater acoustic communications.

Do Young Kwak received his BS degree in mathematics from Seoul National University, Rep. Korea in 1977, and his PhD in mathematics from the University of Pittsburgh, Pittsburgh, Pennsylvania, USA in 1985. From 1985 to 1990, he was an assistant professor of the Department of Mathematics, Korea Institute of Technology, and from 1990 to 1996, he was an associate professor of the Department of Mathematics, Korea Advanced Institute of Science and Technology (KAIST). Since 1996, he has been a professor of the Department of Mathematical Sciences, KAIST, Daejeon, Rep. of Korea. He has served as the chairman of DMS during 1999–2001. His main research interests include finite element methods, multigrid methods, and other numerical methods to solve partial differential equations

Jiwon Jung received his BS, MS, and PhD degrees in electronic engineering from Sungkyunkwan University, Seoul, Republic of Korea, in 1989, 1991, and 1995, respectively. From November 1990 to February 1992, he was with the LG Research Center, Anyang, Republic of Korea. From September 1995 to August 1996, he was with Korea Telecom, Seoul, Republic of Korea. From August 2001 to July 2002, he was an invited researcher with the Communication Research Center Canada (supported by Natural Sciences and Engineering Research Council of Canada (NSERC)), Ottawa, Canada. Since 1996, he has been with the Department of Radio Communication Engineering, Korea Maritime and Ocean University, Busan, Republic of Korea, where he is now a professor. His main research interests include channel coding theory, digital broadcasting systems, and underwater acoustic communications.

Ki-Man Kim received his BS, MS, and PhD degrees in electronic engineering from Yonsei University, Seoul, Republic of Korea, in 1988, 1990, and 1995, respectively. He was a fellow at Yonsei Medical Center, Seoul, Republic of Korea from 1995 to 1996. Since 1996, he has been with the Department of Radio Communication Engineering, Korea Maritime and Ocean University, Busan, Republic of Korea, where he is now a professor. His main research interests include array signal processing, underwater acoustic/laser communications, and sonar localization.

APPENDIX A

Exact restoring matrix X

From (15), we find a matrix $\mathbf{X}$ satisfying the following relation

$$\begin{bmatrix} \mathbf{G}_{cp} \\ \mathbf{G}_{c} \end{bmatrix} \mathbf{X} = \begin{bmatrix} \mathbf{P}_{cp} \\ \mathbf{P} \end{bmatrix}. \tag{A-1}$$

This matrix equation can be separated into two equations:

$$\mathbf{G}_{cp}\mathbf{X} = \mathbf{P}_{cp}, \tag{A-2}$$

$$\mathbf{G}_{c}\mathbf{X} = \mathbf{P}. \tag{A-3}$$

If (A-3) is satisfied, (A-2) is also satisfied, and thus $\mathbf{X}$ can be obtained using (A-1) as

$$\mathbf{X} = \mathbf{G}_{c}^{+}\mathbf{P}, \tag{A-4}$$

where $\mathbf{G}_{c}^{+}$ is the pseudoinverse of $\mathbf{G}_{c}$.

APPENDIX B

Another restoring matrix X

Multiplying both sides by their complex conjugated matrices, we have

$$\left(\mathbf{G}_{c}\mathbf{X}\right)^{\mathrm{H}} \mathbf{G}_{c}\mathbf{X} = \mathbf{P}^{\mathrm{H}}\mathbf{P}. \tag{B-1}$$

The right term of (B-1) can be rewritten as

$$\begin{aligned} \mathbf{P}^{\mathrm{H}}\mathbf{P} &= \left(\mathbf{F}_{N}^{\mathrm{H}}\mathbf{J}\right)^{\mathrm{H}} \mathbf{F}_{N}^{\mathrm{H}}\mathbf{J} \\ &= \mathbf{J}^{\mathrm{H}}\mathbf{F}_{N}\mathbf{F}_{N}^{\mathrm{H}}\mathbf{J} \\ &= \mathbf{J}^{\mathrm{H}}\mathbf{J} \\ &= \mathbf{I}. \end{aligned} \tag{B-2}$$

Substituting (B-2) into (B-1), we have

$$\mathbf{X}^{\mathrm{H}}\mathbf{G}_{c}^{\mathrm{H}}\mathbf{G}_{c}\mathbf{X} = \mathbf{I}. \tag{B-3}$$

Rearranging for $\mathbf{X}$, (B-3) becomes

$$\begin{aligned} \mathbf{G}_{c}^{\mathrm{H}}\mathbf{G}_{c} &= \left(\mathbf{X}^{\mathrm{H}}\right)^{-1} \mathbf{I}\,(\mathbf{X})^{-1}, \\ \left(\mathbf{X}\mathbf{X}^{\mathrm{H}}\right)^{-1} &= \mathbf{G}_{c}^{\mathrm{H}}\mathbf{G}_{c}. \end{aligned} \tag{B-4}$$

Taking inverse on both side terms yields

$$\mathbf{X}\mathbf{X}^{\mathrm{H}} = \left(\mathbf{G}_{c}^{\mathrm{H}}\mathbf{G}_{c}\right)^{-1}. \tag{B-5}$$

Letting $\mathbf{X}$ be Hermitian, (B-5) can be written as

$$\mathbf{X}^{2} = \left(\mathbf{G}_{c}^{\mathrm{H}}\mathbf{G}_{c}\right)^{-1}, \tag{B-6}$$

$$\mathbf{X} = \pm\left(\mathbf{G}_{c}^{\mathrm{H}}\mathbf{G}_{c}\right)^{-\frac{1}{2}}. \tag{B-7}$$

In this paper, we choose the positive solution

$$\mathbf{X} = \left(\mathbf{G}_{c}^{\mathrm{H}}\mathbf{G}_{c}\right)^{-\frac{1}{2}}. \tag{B-8}$$

APPENDIX C

Approximating $\mathbf{G}_c$ in the frequency domain, $\hat{\Psi}$

The frequency domain representation of $\mathbf{G}_c$ is

$$\begin{aligned}\Psi &= \left[\boldsymbol{\psi}_1, \boldsymbol{\psi}_2, \ldots, \boldsymbol{\psi}_M\right]_{N\times M} \\ &= \left[\mathbf{F}_{N+2}\mathbf{G}_c\right]_{N\times M},\end{aligned} \tag{C-1}$$

where each entry is represented as

$$\begin{aligned}\boldsymbol{\psi}_i &= \left[\left(\mathbf{F}_{N+2}\mathbf{c}\right)\left(\mathbf{F}_{N+2}\mathbf{q}_i\right)\right]_{N\times 1} \\ &= \left[\mathbf{F}_{N+2}\mathbf{c}\right]_{N\times 1}\left[\mathbf{F}_{N+2}\mathbf{q}_i\right]_{N\times 1} \\ &= \boldsymbol{\gamma}\boldsymbol{\rho}_i\end{aligned} \tag{C-2}$$

where

$$\boldsymbol{\gamma} = \left[\mathbf{F}_{N+2}\mathbf{c}\right]_{N\times 1}, \tag{C-3}$$

$$\boldsymbol{\rho}_i = \left[\mathbf{F}_{N+2}\mathbf{q}_i\right]_{N\times 1}. \tag{C-4}$$

All entries of $\boldsymbol{\gamma}$ are nonzero and $[\mathbf{a}]_{N\times 1}$ denote the $N\times 1$ size-reduced vector by removing the first and last entries of $(N+2)\times 1$ vector $\mathbf{a}$. When $N \gg 2$, because the values of neighboring entries are very similar to the value of the current location, (C-4) can be rewritten approximately as

$$\begin{aligned}\boldsymbol{\rho}_i &\approx \mathbf{F}_N\left[\mathbf{q}_i\right]_{N\times 1} \\ &= \mathbf{F}_N\mathbf{p}_i \\ &= \mathbf{J}_i,\end{aligned} \tag{C-5}$$

where $\mathbf{J}_i$ is the i-th column vector of the mapping matrix $\mathbf{J}$.

The approximated matrix of Ψ is defined as

$$\hat{\Psi} = \left[\gamma\mathbf{J}_1, \gamma\mathbf{J}_2, \ldots, \gamma\mathbf{J}_M\right]. \tag{C-6}$$

From (1), $\mathbf{J}_i$ has only an entry with 1, the matrix $\hat{\Psi}$ can be rewritten as

$$\hat{\Psi} = \begin{bmatrix}\mathbf{0}_{1\times M} \\ \mathbf{A} \\ \mathbf{0}_{\beta\times M} \\ & \mathbf{B}\end{bmatrix}, \tag{C-7}$$

where

$$\mathbf{A} = \begin{bmatrix}\gamma_1 & & & \\ & \gamma_2 & & \\ & & \ddots & \\ & & & \gamma_{M/2}\end{bmatrix}, \tag{C-8}$$

$$\mathbf{B} = \begin{bmatrix}\gamma_{N+2-M/2+1} & & & \\ & \gamma_{N+2-M/2+2} & & \\ & & \ddots & \\ & & & \gamma_{N+2}\end{bmatrix}, \tag{C-9}$$

and γ_i is the i-th entry of $\boldsymbol{\gamma}$.

APPENDIX D

Approximating the restoring matrix

Substituting (21) into (17), we have

$$\begin{aligned}\mathbf{X} &\approx \left(\begin{bmatrix}\mathbf{0}_{1\times M} \\ \mathbf{A} \\ \mathbf{0}_{\beta\times M} \\ & \mathbf{B}\end{bmatrix}^{\mathrm{H}}\begin{bmatrix}\mathbf{0}_{1\times M} \\ \mathbf{A} \\ \mathbf{0}_{\beta\times M} \\ & \mathbf{B}\end{bmatrix}\right)^{-\frac{1}{2}} \\ &= \left(\begin{bmatrix}\mathbf{0}_{M\times 1}\,\mathbf{A}^{\mathrm{H}}\,\mathbf{0}_{M\times\beta} & \\ & \mathbf{B}^{\mathrm{H}}\end{bmatrix}\begin{bmatrix}\mathbf{0}_{1\times M} \\ \mathbf{A} \\ \mathbf{0}_{\beta\times M} \\ & \mathbf{B}\end{bmatrix}\right)^{-\frac{1}{2}} \\ &= \begin{bmatrix}\mathbf{A}^{\mathrm{H}}\mathbf{A} & \mathbf{0} \\ \mathbf{0} & \mathbf{B}^{\mathrm{H}}\mathbf{B}\end{bmatrix}^{-\frac{1}{2}}.\end{aligned} \tag{D-1}$$

As $\mathbf{A}$ and $\mathbf{B}$ are diagonal, $\mathbf{X}$ can be written as

$$\mathbf{X} \approx \begin{bmatrix}\left(\mathbf{A}^{\mathrm{H}}\mathbf{A}\right)^{-\frac{1}{2}} & \mathbf{0} \\ \mathbf{0} & \left(\mathbf{B}^{\mathrm{H}}\mathbf{B}\right)^{-\frac{1}{2}}\end{bmatrix}. \tag{D-2}$$

When $r = 2$, because the zero-insertion filter is an even function, the elements of $\mathbf{A}$ and $\mathbf{B}$ are real in the frequency domain. Therefore, $\mathbf{X}$ can be reduced to:

$$\mathbf{X} \approx \begin{bmatrix}\mathbf{A}^{-1} & \mathbf{0} \\ \mathbf{0} & \mathbf{B}^{-1}\end{bmatrix}. \tag{D-3}$$

APPENDIX E

Vectorization

The vector $\mathbf{X}\,\mathbf{d}$ can be written as

$$\begin{aligned}\mathbf{u} &= \mathbf{X}\mathbf{d} \\ &= \mathbf{x} \odot \mathbf{d},\end{aligned} \tag{E-1}$$

where $\odot$ is the element-wise product operator and the vector $\mathbf{x}$ is represented as

$$\mathbf{x} = \mathrm{diag}(\mathbf{X}). \tag{E-2}$$

Because $\mathbf{J}$ is a data symbol loading matrix, there is no actual multiplication, we leave it as follows:

$$\begin{aligned}\mathbf{v} &= \mathbf{J}\mathbf{u} \\ &= \mathbf{J}\mathbf{x} \odot \mathbf{d}.\end{aligned} \tag{E-3}$$

Because $\mathbf{F}_N^{\mathrm{H}}$ is the IDFT matrix, it can be replaced with an IFFT operator as

$$\begin{aligned}\mathbf{p} &= \mathbf{F}_N^{\mathrm{H}}\mathbf{v} \\ &= \mathbf{F}_N^{\mathrm{H}}\mathbf{J}\mathbf{x} \odot \mathbf{d}.\end{aligned} \tag{E-4}$$

Because $\mathbf{E}$ is a permutation matrix, there is no actual multiplication, so we leave it as follows:

$$\begin{aligned}\mathbf{q} &= \mathbf{E}\mathbf{p} \\ &= \mathbf{E}\,\mathbf{F}_N^{\mathrm{H}}\mathbf{J}\mathbf{x} \odot \mathbf{d}.\end{aligned} \tag{E-5}$$

Because $\mathbf{W}$ is a diagonal matrix, the matrix product is represented as

$$\begin{aligned}\mathbf{r} &= \mathbf{W}\mathbf{q} \\ &= \mathbf{W}\mathbf{E}\,\mathbf{F}_N^{\mathrm{H}}\mathbf{J}\mathbf{x} \odot \mathbf{d} \\ &= \mathbf{w}\mathbf{E}\,\mathbf{F}_N^{\mathrm{H}}\mathbf{J}\mathbf{x} \odot \mathbf{d},\end{aligned} \tag{E-6}$$

where

$$\mathbf{w} = \mathrm{diag}(\mathbf{W}). \tag{E-7}$$

Because $\mathbf{C}$ is a convolution matrix, vector $\mathbf{s}$ is represented as

$$\begin{aligned}\mathbf{s} &= \mathbf{C}\mathbf{r} \\ &= \mathbf{c} * \mathbf{r} \\ &= \mathbf{c} * \left(\mathbf{w}\mathbf{E}\,\mathbf{F}_N^{\mathrm{H}}\mathbf{J}\mathbf{x} \odot \mathbf{d}\right).\end{aligned} \tag{E-8}$$